

**STUDIES ON LAMINAR AND TURBULENT REYNOLDS NUMBER FOR  
STANDARDIZED NASAL CAVITY**

By:

**FOO KAR YEN**

(Matrix No: 120556)

Supervisor:

**DR. NORIZHAM BIN ABDUL RAZAK**

JUNE 2017

This dissertation is submitted to

Universiti Sains Malaysia

as partial fulfillment of the requirement to graduate with honors degree in

**BACHELOR OF ENGINEERING (AEROSPACE ENGINEERING)**



School of Aerospace Engineering

Engineering Campus

Universiti Sains Malaysia

**DECLARATION**

This work has not previously been accepted in substance for any degree and is not being concurrently submitted in candidature for any degree.

Signed .....

(FOO KAR YEN)

Date: 5<sup>th</sup> June 2017

**STATEMENT 1**

This paper is the results of my own investigations, except where otherwise stated. Other sources are acknowledged by giving explicit references. Bibliography/references are appended.

Signed .....

(FOO KAR YEN)

Date: 5<sup>th</sup> June 2017

**STATEMENT 2**

I hereby give consent for my paper, if accepted, to be available for photocopying and for interlibrary load, and for the title and summary to be made available to outside organization.

Signed .....

(FOO KAR YEN)

Date: 5<sup>th</sup> June 2017

# STUDIES ON LAMINAR AND TURBULENT REYNOLDS NUMBER FOR STANDARDIZED NASAL CAVITY

*Norizham Abdul Razak, Chih Fang Lee, and Kar Yen Foo*

**Abstract** – The airflow dynamics of a human nasal cavity is as important as its physiological functions, yet these dynamics are not well known. Numbers of features in nose have been argued to enhance airflow turbulence, thus increasing the heat exchange, humidifying inhaled air and greater exposure of moving air to nasal mucosa [1]. In conjunction to that, the flow regimes (laminar, transitional or turbulent) are studied in order to correlate the nasal morphology and turbulent airflow. Previous researchers mentioned that Reynolds number below 2000 is said to be laminar flow, while higher than that indicates turbulent flow. However, this is partially true because the flow is assumed to be in a straight, smooth-walled pipe. Hence, CFD simulation is carried out to further investigate the airflow patterns at varying flow rates. Laminar model is used to run the simulation for flow rates of 4.5 L/min, 7.5 L/min, 10 L/min and 15 L/min, while a two equation turbulence model, shear stress transport (SST)  $k-\omega$  is adapted for flow rate of 18 L/min. Velocity magnitudes, velocity contours, velocity vectors and streamlines are collected for analysis. Besides that, experimental work using PIV is adapted as well in order to evaluate the flow characteristics in a model of human nasal cavity. The overall results suggested that airflow turbulence begin at flow rate of 18 L/min, where swirling and twisting flows are found at few regions. The aid of CFD and PIV allows better understanding and visualization of the airflow pattern in human nasal cavity.

## Table of Contents

Abstract.....	ii
1.0 Introduction .....	1
1.1 Research Background.....	1
1.2 Problem Statement.....	2
2.0 Literature Review .....	2
2.1 Computational Analysis .....	2
2.1.1 Geometrical Modelling .....	2
2.2 Experimental Studies .....	3
2.2.1 Experimental Model.....	3
2.2.2 Reynolds Number Distribution in Nasal Airway.....	4
2.2.3 Particle Image Velocimetry (PIV) .....	4
2.2.4 Tracer Particles and Seeding for PIV .....	5
3.0 Methodology.....	5
3.1 Computational Analysis .....	6
3.1.1 Modification of Nasal Model Geometry .....	6
3.1.2 Mesh Creation.....	6
3.1.3 Grid Independence Study .....	7
3.1.4 CFD Simulation .....	7
3.1.5 Solution .....	8
3.2 Experimental Works.....	8
3.2.1 Experimental Set-Up .....	9
3.2.2 Selection of Seeding Particles .....	10

4.0 Results and Discussion .....	10
4.1 Computational Comparison .....	10
4.1.1 Average Velocity Magnitude .....	11
4.1.2 Velocity Contours .....	12
4.1.3 Velocity Streamlines .....	12
4.2 Experimental Comparison .....	15
5.0 Conclusion .....	17
6.0 Future Recommendation .....	17
Acknowledgement .....	17
Reference .....	18

## List of Figures

<i>Figure 1: (a) Anatomy of a nasal cavity and (b) coronal section in the main nose airway</i> .....	1
<i>Figure 2: (a) Nose-like model and (b) Nasal model with addition of inlet tube and extended nasopharynx</i> .....	3
<i>Figure 3: Nasal model using rapid prototyping technique</i> .....	3
<i>Figure 4: Human plastinated specimen of nasal cavity</i> .....	3
<i>Figure 5: General schematic of experimental setup for PIV</i> .....	5
<i>Figure 6: Flow chart of methodology</i> .....	5
<i>Figure 7: 3D model created by Lee</i> .....	6
<i>Figure 8: Final model created after modification process</i> .....	6
<i>Figure 9: Mesh creation of nasal model</i> .....	7
<i>Figure 10: Boundary conditions</i> .....	7
<i>Figure 11: Velocity magnitudes for standardized half-model with mass flow rate 7.5 L/min</i> .....	7
<i>Figure 12: Cut planes: A = Vestibule, B = Nasal Valve, C = Middle Plane, D = Nasopharynx</i> .....	8
<i>Figure 13: Coordinate reference axes</i> .....	8
<i>Figure 14: Nasal model from Lee</i> .....	9
<i>Figure 15: (above) Real experimental set-up: (1) HiSense Camera, (2) Computer system, (3) Nd:YAG Laser system, (4) Nasal Model, (5) Hydraulic bench and (bottom) Schematic diagram of the experimental set-up</i> .....	10
<i>Figure 16: Average velocity magnitudes at flow rate 7.5 L/min in different cross-sectional planes</i> .....	11
<i>Figure 17: Average velocity magnitudes at flow rate 18 L/min in different cross-sectional planes</i> .....	11
<i>Figure 18: Velocity streamline at flow rate of 7.5 L/min</i> .....	12
<i>Figure 19: Velocity streamline at flow rate of 18 L/min</i> .....	13
<i>Figure 20: Computational velocity vector at flow rate 4.5 L/min</i> .....	15
<i>Figure 21: (a) Computational velocity vectors and (b) Experimental velocity vectors at flow rate 4.5 L/min</i> .....	15
<i>Figure 22: Laser profile misalignment</i> .....	<b>Error! Bookmark not defined.</b>

## List of Tables

<i>Table 1: Literature survey of airflow simulations and the flow regime .</i>	4
<i>Table 2: Tracer particles used by previous researchers.</i>	5
<i>Table 3: Grid independence studies</i>	7
<i>Table 4: Types of seeding particles by Lee</i>	10
<i>Table 5: Velocity contour for flow rate of 7.5 L/min and 18 L/min</i>	12
<i>Table 6: Literature survey of airflow regime</i>	13
<i>Table 7: Streamline pattern for two regions in different flow rates</i>	14
<i>Table 8: Reynolds number calculated corresponding to the flow rate.</i>	15

## Abbreviations

CFD	Computational Fluid Dynamics
PIV	Particle Image Velocimetry
Re	Reynolds Number
$Q$	Flow rate of fluid
$D$	Diameter of pipe
$\nu$	Kinematic viscosity of flowing fluid
$A$	Cross sectional area of pipe

## 1.0 Introduction

### 1.1 Research Background

Airflow in human nose is crucial for many physiological functions, specifically warming and humidifying inhaled air, filtering airborne pollutants, and olfaction [2]. The nasal cavity consists of two distinct air passages which are nominally symmetric and is separated by a thin wall called nasal septum [3]. Referring to Figure 1, there are three turbinates or known as conchae (inferior, middle, and superior) and they are separated by meatuses into parallel channel along the septum. High nasal airflow is seen along the nasal floor, followed by middle meatus and there is only 5% to 15% of the total inspiratory nasal airflow that reaches the superior meatus [2]. Figure 1(a) also shows the entrance of air from nostril to the nasopharynx. Air enters the nasal cavity through the nostril and passes the narrowest passage called nasal valve in which the constrict area causes increase in speed. While along the middle and posterior region of the nasal cavity, the air decelerated due to the expansion of area. At the end of the main airway and beginning of nasopharynx, both left and right nasal cavities merged, hence promoting vortices.

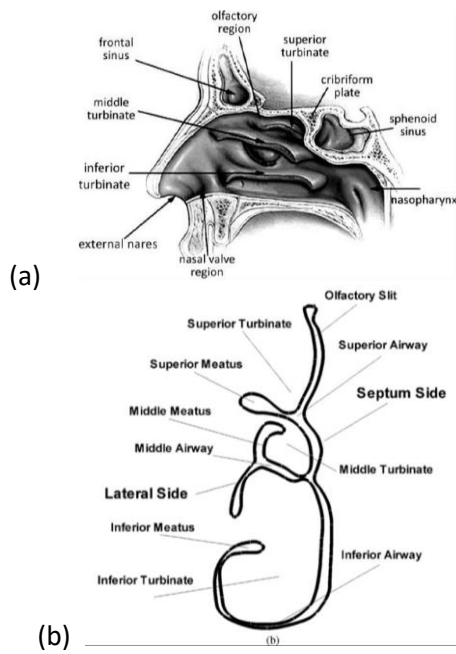


Figure 1: (a) Anatomy of a nasal cavity and (b) coronal section in the main nose airway [4, 5]

Airflow profiles in human nasal cavity have been studied experimentally by several researches. Churchill et al. studied on an anatomically accurate acrylic human nasal model using water and dye. Different flow rates were examined whether the flow is laminar, transition or turbulent. Laminar flow is set to be below Reynolds number ( $Re$ ) of 2000 and is not conducive to air modification and filtration functions due to lower moisture gradient. Where  $Re$  above 2000 is known as turbulent flow, maintains a steep moisture gradient, increases the rapidity of heat and mass transfer and enhances particle filtration and removal of soluble gases [1].

Numerous studies were conducted on human nasal cavity via CFD, constructed from CT or MRI images. CFD simulation enables the complex structure to be quantitatively measured, and visually captured, the flow regimes (laminar, transition or turbulent), velocity, pressure, wall shear stress, particle deposition, and temperature changes at different flow rates and in different regions of nasal cavity. With the current advancing CFD technology, more promising outcomes will be developed [6]. Meanwhile, Wen et al. conducted studies on airflow pattern using computational fluid dynamics (CFD) for a steady-state flow. Analysis was performed with constant flow rates of 7.5 L/min and exercise 40 L/min and resulted in  $Re$  of 545 and 2905 respectively [6].

Kelly et al. also investigated the two-dimensional velocity fields in parallel planes to the flow pattern through nasal model (constructed from 26 CT scans) using particle image velocimetry (PIV) subjected to a non-oscillatory flow rate of 7.5 L/min. The result shows that flow is laminar and high velocity flow is observed in nasal valve and inferior airways, while low flow presents in olfactory region as well as meatuses [7]. The same method was adapted by Doorly et al. and Seung-Kyu et al. in understanding the airflow properties and the development of flow instability in the transparent model or 3-D printed model of nasal cavity [8, 9]. Also, Hopkins et al. did research on PIV on complex geometries over two- or three-dimensional domains. PIV measures the fluid velocities in a transparent material. The flow is

then mixed with seeding particles and is illuminated with laser light. However, it is limited by the inability to fabricate an accurate, transparent replicate the complex model of passage. Hence, a new method namely rapid prototyping technique is introduced to overcome the problem faced [10].

The main focus of this project is to conduct computational analysis via CFD to study and identify the flow regimes in human nasal cavity. Experimental studies are also performed to visualize laminar and turbulent flow for the model of human nasal cavity. The processes include modification of design, running CFD simulation and the conduct of experiment. The flow regimes along the nasal airway are examined through experimental works utilizing PIV and computational analysis via ANSYS.

### **1.2 Problem Statement**

Previous researchers have implemented that the flow inside a straight, smooth-walled pipe is said to be laminar at  $Re < 2000$ , while is turbulent at  $Re > 2000$ . This flow regime was set as the guidelines so that experimental results can be compared. At Reynolds number below 2000, the viscous forces operating on the fluid are sufficient to dampen disturbances created by inertial forces, thus the flow remains laminar [1]. Nevertheless, this condition only applies to narrow circumstances where the flow occurs in a straight, rigid, dry, and smooth-walled pipes. Divergence from the ideal conditions will increase the inertial disturbances and apparently disrupt the laminar flow. The disturbances will eventually increase with flow velocity but during quiet breathing the characteristics of the structurally intricate airways are not conducive to laminar flow. According to Schreck et. al., the flow in an anatomically accurate nasal model is described to be transition to turbulence at Reynolds number approximate 600 [11]. Features like nostril orientation, nasal valve size, nasal still height, and position of the turbinates play important roles in the production of airflow turbulence since the four features deviate from the characteristics of a straight, smooth-walled, and uniform pipe. Due to the

short length, complex and curvaceous nasal cavity, the Reynolds number is not necessarily the same as experimentally determined value for flow through a straight, smooth cylinder. Hence, the traditional definition for the transitional flow regime are not completely applicable in nasal airflow studies. In conjunction to that, a new standard Reynolds number that differentiate laminar and turbulent in nasal airways is yet to be identified. Hence, the currently leading experimental tool, PIV will be used for this project to visualize and understand the airflow pattern in model of human nasal cavity. To validate the results obtained, CFD simulation via ANSYS FLUENT is conducted.

## **2.0 Literature Review**

### **2.1 Computational Analysis**

The recent developments in medical imaging, three-dimensional geometry modelling and numerical mathematics provides large advancement in technology where the human nasal model can be portrayed precisely in computer for computational analysis [12]. CFD method is applied widely in science and industry to design and optimize products and to simulate natural processes, including numerous biomedical applications [12]. In order to study and understand the detailed flow patterns inside the human nasal cavity without any intervention or clinical risk to patient, CFD is implemented.

#### **2.1.1 Geometrical Modelling**

To date, an anatomically accurate numerical model of human nasal cavity is not available [13]. Hence, only identical models with slight modifications for simplification purpose are adapted. Most of the previous researchers constructed the models from CT or MRI scans images using MIMICS software, namely Dohare et al., Lee et al., Zubair et al., and Chen et. al. [4, 14-16]. The scans should include entire nose from nostril to posterior wall of nasopharynx because if these extremes are not included, the direction of flow in and flow out will be not be modelled, leading to a potentially unrealistic airflow in nasal

cavity [17]. Elad et al. conducted a numerical simulation on a “nose-like” model using finite-element method via FIDAP package (Fluid Dynamics International) [18]. Meanwhile, Shi et al. made few modifications on its nasal model by adding a short inlet tube to each nostril to avoid plug flow entering the nostrils, and a certain length of actual airway was added to nasopharynx to obtain proper outlet conditions [19].

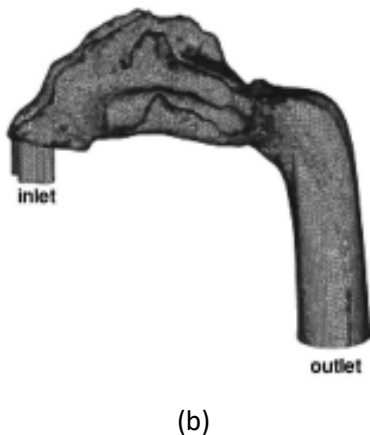
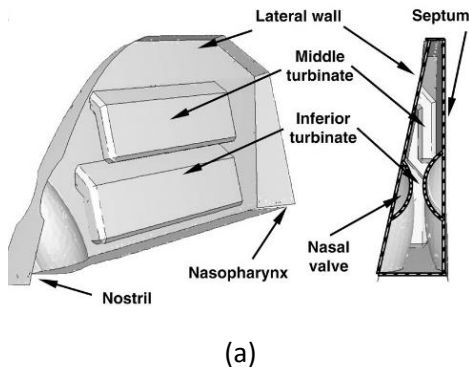


Figure 2: (a) Nose-like model [18] and (b) Nasal model with addition of inlet tube and extended nasopharynx [19]

## 2.2 Experimental Studies

### 2.2.1 Experimental Model

Nasal cavity is small and structurally complex and these factors has prevented detailed in vivo experimental studies of nasal airflow. Hence, numerous in vitro studies on 3-D models from CT scans have been carried out. However, the resolution and quantitative accuracy in measurement of experimental studies are still lagging behind. With the advancement of CFD techniques, the nasal airflow can be simulated

within numerically constructed, anatomically accurate models [2]. Experiment setup such as PIV encountered difficulties in replicating complex geometries with optically transparent material. Hence, Hopkins et al. as well as Kim et al. developed a rapid prototyping technique in which model is generated in water-soluble consolidated cornstarch to remove unwanted parts [10, 20]. Besides, due to the demanding complexity of the nasal airways, Croce et al. choses to study the human nasal cavity using human plastinated specimen because it provides realistic perspective. The anatomical specimen undergoes processes including fixation, dehydration, forced impregnation, and polymerization – a well-known technique for anatomical conservation [21]. Meanwhile, Hahn et al. did a large scale (X20) anatomically correct model, constructed from CAT scans in order to overcome the limitation of studies in a small size and complicated anatomy [22].

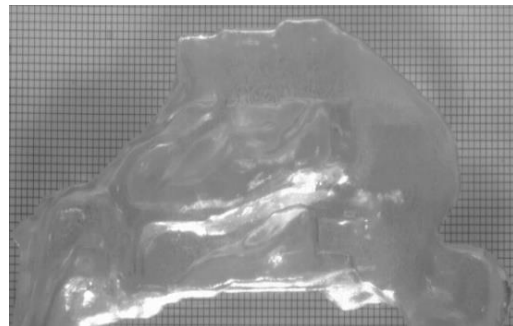


Figure 3: Nasal model using rapid prototyping technique [10]

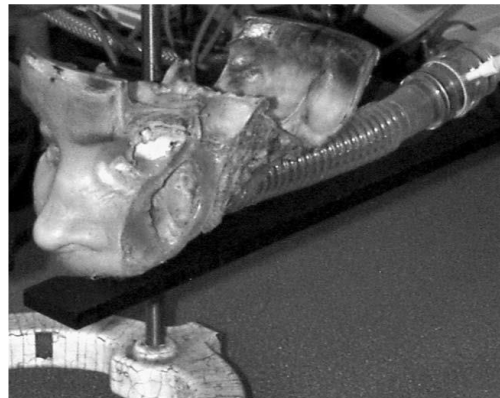


Figure 4: Human plastinated specimen of nasal cavity [21]



### 2.2.2 Reynolds Number Distribution in Nasal Airway

Over the past decades, researchers have been developing ways (laser Doppler velocimetry, CAT, MRI, water and dye, CFD, PIV, hot wire anemometer, etc.) in exploring the nasal airways. In a smooth-walled pipe, the characteristic of fluid flow, whether it is laminar, transition or turbulent is entailed of fluid density, viscosity, flow velocity, and the size of pipe [1]. All these factors contribute to a dimensionless value, Reynolds number ( $Re$ ), which defines as the ratio of inertial forces to viscous forces and is used to identify the flow velocity at which turbulence will occur.

Laminar flow occurs for low Reynolds number, with relatively slow flow velocity and high viscosity. It is characterized by all the fluid velocity vectors lined up in the direction of flow. On the other hand, turbulent flow occurs at high Reynolds number, with relatively high flow velocity and low viscosity. It has point vectors in all directions, although the overall flow is in one direction, along the axis of the pipe. At Reynolds number less than 2000, the viscous forces operating on the fluid is sufficient to weaken the disturbances created by inertial forces, thus flow remains laminar. However, it only applies flow regimes with continuous flow on straight, rigid, dry, smooth-walled pipes [1]. The method to determine whether the flow is laminar or turbulent is the value of the Reynolds number. The Reynolds number can be defined as:

$$Re = \frac{QD}{\nu A}$$

Where,

$$Q = \text{flow rate of fluid} \left( \frac{m^3}{s} \right)$$

$$D = \text{diameter of pipe (m)}$$

$$\nu = \text{kinematic viscosity of flowing fluid (m}^2/\text{s)}$$

$$A = \text{cross sectional area of pipe (m}^2\text{)}$$

Churchill et al. mentioned that Reynolds below 2000 is said to be laminar flow while Reynolds

number beyond that will be turbulent flow [1]. There will also be transition region between the two regime, depending upon the nature of the entrance to the pipe and the pipe wall roughness. Table 1 below shows the respective data collected based on the researchers.

Table 1: Literature survey of airflow simulations and the flow regime [6]

Researchers	Flow Rate (L/min)	Reynolds Number
Afiza et. al. [23]	-	880
Zamankhan et. al. [5]	14	490
Dombrowski [24]	6	462
Croce et. al. [21]	15	1250
Spence et. al. [25]	22	1530
Stringer et. al. [26]	22	1760

### 2.2.3 Particle Image Velocimetry (PIV)

Particle Image Velocimetry (PIV) is a powerful tool which is able to determine the instantaneous flow field over two- or three-dimensional domains. The flow passage is fabricated using optically transparent material. Fluid that is seeded with tracer particles will then flow through the passage and is illuminated with a sheet of laser light. By pulsing the laser twice in rapid succession, two subsequent positions of the particles are recorded. Post-processing generates two- or three-dimensional instantaneous velocity vector while translational sheet will yield full three-dimensional nature [10]. With the known displacements, the time between the two successive illuminations and magnification factor, the velocity field can be calculated [27]. Figure 5 shows the general schematic arrangement of an experimental PIV setup in a wind tunnel.

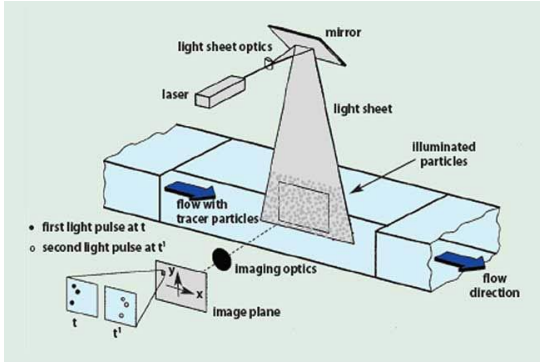


Figure 5: General schematic of experimental setup for PIV [27]

Regarding the variety of fluid used in PIV, experimental medium is an important factor which contributes to the accuracy of results. Hopkins et al. found out that a mixture of 59% glycerol and 41% water is the optimal proportion by volume. This mixture of their matching eliminates the distortion of light scattered from the particles and refraction of the laser sheet as fluid passes through the flow passage [10]. Other than that, researchers like Croce et al. prefer to use gases; Heliox (gas mixture containing 65% He and 35% O<sub>2</sub>), room air, and Sulphur Hexafluoride (SF<sub>6</sub>) [21].

#### 2.2.4 Tracer Particles and Seeding for PIV

Methods like PIV and Laser Doppler Anemometry (LDA) rely solely on scattering particles seeded in flow to provide velocity information for the continuous medium. The accuracy of the velocity field determination is ultimately limited by the ability of the scattering particles to follow instantaneous motion of the continuous phase [28]. Below are few examples of tracer particles used by previous researchers.

Table 2: Tracer particles used by previous researchers

Researchers	Tracer particles used
Hopkins et al., 2000[10]	60 μm hollow glass sphere
Nayebossadri, 2012[27]	Olive oil
Afiza et al., 2015[23]	Orgasol polyamide powder
Kelly et al., 2000[7]	60 μm hollow glass sphere

Spence et al., 2011[25]	10 μm hollow glass sphere
Lee, 2014[29]	50 μm hollow glass sphere

### 3.0 Methodology

The overall methodology for this project is described as follow and is depicted in the flow chart below. The experiment will begin with the modification on the existing model developed by Lee [29]. Previous 3-D model developed possesses some rough and inaccurate surface, hence the geometry is required to undergo smoothing and refining process using CATIA V5. Next the modified model is used to undergo simulations by adapting ANSYS FLUENT 6.3.26 (Fluent, Lebanon, USA) to collect and analyze data. Then experimental works will be carried out adapting the existing model created by Lee as shown in Figure 6. PIV is set-up using appropriate seeding material, medium and setting of velocity. The results obtained is then compared with the existing sources or references and computational studies for validation purpose.

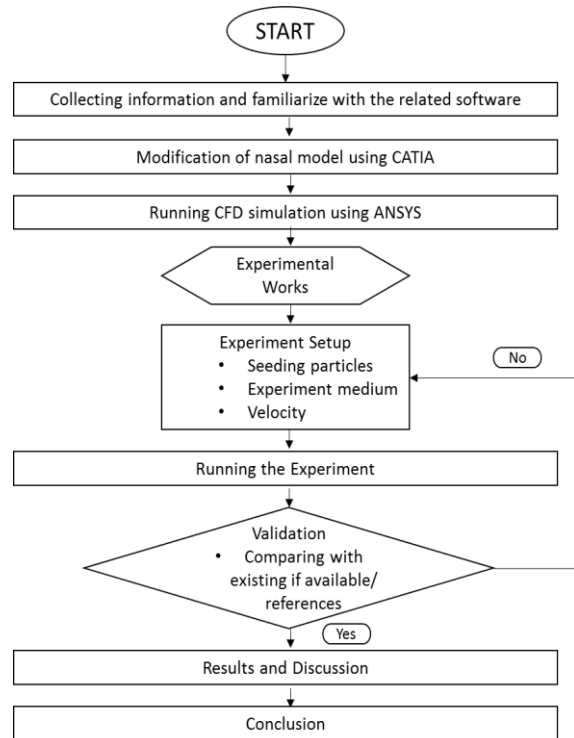


Figure 6: Flow chart of methodology

### 3.1 Computational Analysis

#### 3.1.1 Modification of Nasal Model Geometry

The 3D nasal model is already existed which is first created by Lee as shown in Figure 7. The model has rough surfaces which will cause inaccurate results obtained. Hence, it is advisable to smoothen and refine the rough surface of the model for better results. This step is done by using CATIA V5 via Digitized Shape Editor Workbench. Few tools are used including removing interactive triangle, deleting unwanted sharp edges, and smoothening rough regions through mesh creation. A final model with lesser number of surfaces is created after mass modification is done. The image of the final model is portrayed in Figure 8 below.

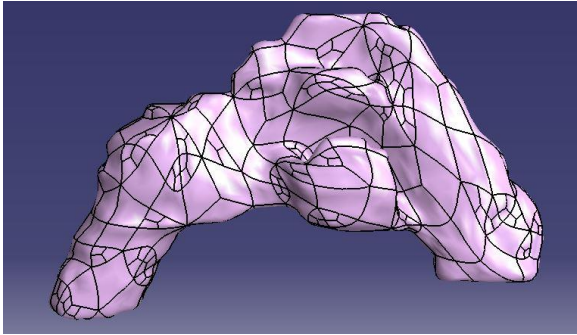


Figure 7: 3D model created by Lee [29]

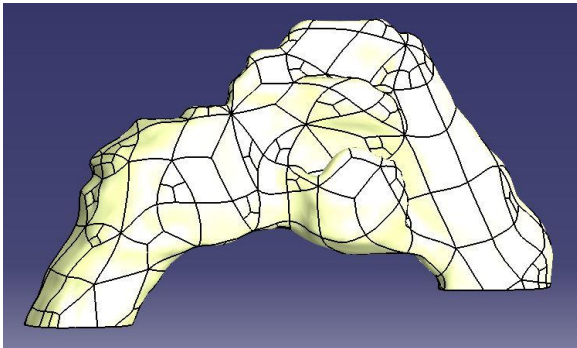


Figure 8: Final model created after modification process

Half-model is cut from the standardized model so that comparison can be made with models obtained from Lee, Wen et al. and Zubair et al. [6, 15, 29]. The final model is then saved in STEP file so that it can be imported to ANSYS Workbench 16.0 to carry out volume meshing process.

#### 3.1.2 Mesh Creation

The meshing process is carried out in ANSYS Workbench 16.0 via ANSYS Mechanical. In order to analyze fluid flows, meshing process is a necessity. The mesh generation is a decisive stage in obtaining a model that produces good result [30]. It is a process of dividing fluid domains into smaller non-overlapping subdomains. The subdomains are also known as elements or cells, and the combination of all elements or cells is called as mesh. The purpose of meshing is to present detail airflow pattern properly, depicting important features of airflow in the final simulation [17]. There are two types of mesh: structured and unstructured mesh. Structured mesh is grids with regular connectivity, while unstructured mesh is grids with irregular connectivity. In this project, unstructured mesh is adapted since the geometry of the nasal model is complex.

Meshing is important at crucial regions like turbinate inside the nasal cavity. Thus, lack of mesh elements at those areas will eventually cause failure in capturing the nasal airflow [31]. However, too many elements will result in long computation times to obtain the nasal airflow. Therefore, it is essential to make a balance between achieving sufficient amount of mesh density that can exhibit correct results and without increasing much of the computation time [17]. It is a must that the mesh begins and end at definite points which are the inlet and outlet of the nasal airflow simulations [17].

After the generation of mesh elements, the boundary types are required to be figured out in order to define the boundary conditions for flow simulations. There are:

- Inlet – Resemblance of the nostril where flow began when inhalation takes place.
- Outlet – Located at the end of nasopharynx.

- Wall – To define the boundary between inner and outer nasal cavity.

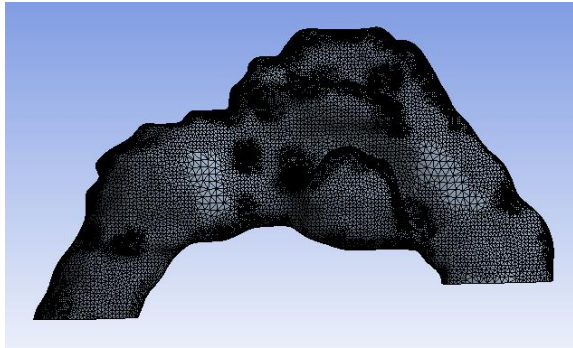


Figure 9: Mesh creation of nasal model

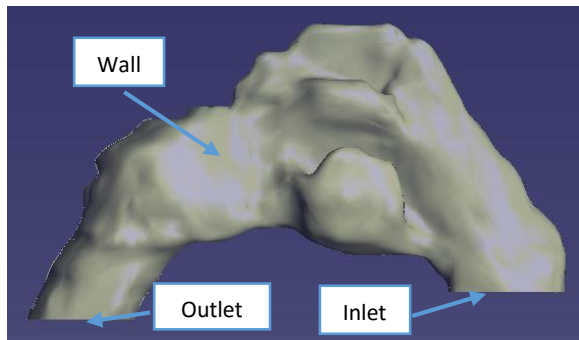


Figure 10: Boundary conditions

### 3.1.3 Grid Independence Study

It is important to reach a compromise between high-resolution meshes, but with longer calculation time, and low-resolution meshes with little calculation time, yet the results produced are not reliable [30]. Therefore, the comparative grid independence studies are carried out in order to establish the minimum resolution of meshing, from which the results are independent of the number of elements [30]. Applying finer meshes means creating smaller volumes of elements or cells, simultaneously increasing the mesh density. This increment in mesh density beyond a critical number of tiny volumes will cause the results to change so little at the point where the errors are negligible [17]. Hence, the results are said to be independent of the mesh density. The unstructured tetrahedral meshing is successfully constructed with the range from 600,000 to 1,000,000 elements.

Table 3: Grid independence studies

	Model 1	Model 2	Model 3
Relevance Center	Coarse	Medium	Fine
Smoothing	Medium	High	High
Growth Rate	1.2	1.18	1.15
No. of Elements	648,512	863,526	1,112,568

The model was improved by element adaptation techniques in order to create a finer mesh at areas where high velocity gradients are found, refining large volumes elements, and near wall refinements [6]. This can be done by manipulating the relevance center, smoothing, and growth rate.

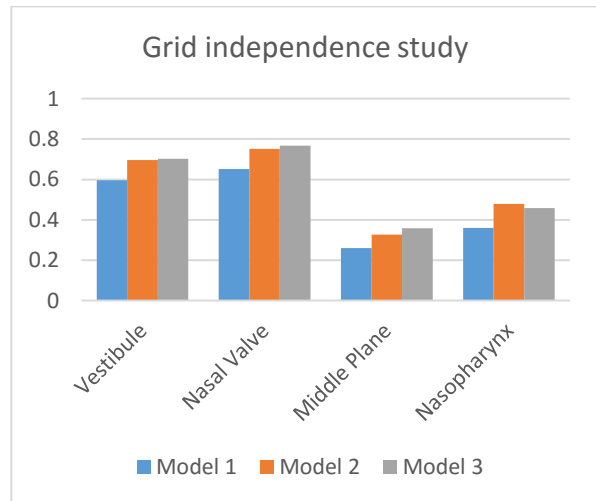


Figure 11: Velocity magnitudes for standardized half-model with mass flow rate 7.5 L/min

The difference between the results obtained from Model 2 and 3 is less as compared to difference between Model 1 and Model 2. Meanwhile, the calculation time for Model 3 is relatively large (two times longer) as compared to Model 2. Hence, by considering both mesh resolution and time concern, Model 2 with 863,526 elements is chosen for the analysis.

### 3.1.4 CFD Simulation

Numerical simulations are conducted on the meshed model via ANSYS FLUENT 6.3.26 (Fluent, Lebanon, USA). The simulation is based on the

numerical solution of the Navier-Stokes equation which portrays the general equation for 3D flow of incompressible and viscous fluids [32]. Laminar model and a two equation turbulence model, SST k- $\omega$  is utilized in this simulation. The suitability of shear stress transport (SST) k- $\omega$  model had been experimentally validated by Wen et al. [6] and Mylavarapu et al. [33]. Besides, the SST k- $\omega$  model can be operated to capture such complex laminar-transitional-turbulent flow inside the nasal cavity [16].

There are few assumptions made in this analysis. First, it is assumed that the flow simulations are conducted at steady-state inspiratory flow, corresponding to resting breathing rate [34]. Secondly, the flow is assumed to be incompressible. The flow with very low Mach number ( $M < 0.3$ ) has justified the assumption of flow incompressibility [33]. Furthermore, a pressure-based solver method is adapted since it has better compatible mode with low-speed incompressible flow [6]. Last but not least, the nasal wall is assumed to be rigid, with no presence of mucus [32].

The boundary conditions which consist of inlet, outlet and nasal wall are defined as follow:

- Inlet – Mass flow inlet
- Outlet – Outflow
- Wall – No-slip boundary

These boundary conditions are defined based on previous works from Riazuddin et al., Zubair et al., and Lee [15, 29, 32].

### 3.1.5 Solution

In this CFD analysis, the mass flow rate used ranges from 4.5 L/min to 18 L/min. Laminar model is adapted for flow rate of 4.5 L/min, 10 L/min, and 15 L/min, while a two equation turbulence model, SST k- $\omega$  is applied to flow rate of 18 L/min. Simulations are carried out for cross-sectional areas along the right nasal cavity as shown in Figure 6 Figure 12. The choice of using half-model is because each of two nasal airways tends to used alternately for short period of time during normal

breathing or relaxed state [14, 35, 36]. Next, the position of cuts is made based on the anatomical features [34]. Plane A which is the Vestibule area, is separated from more posterior regions. Plane B representing Nasal Valve region, is the smallest cross-sectional area along the nasal cavity. Place C known as Middle Plane or turbinate, where inferior, middle and superior turbinate regions are noticeable. Lastly, Plane D, as the Nasopharynx cut, near the termination of the nasal septum.

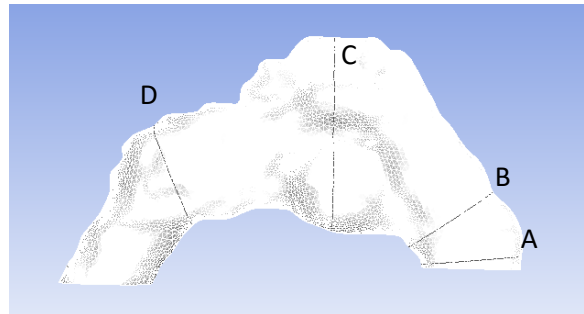


Figure 12: Cut planes: A = Vestibule, B = Nasal Valve, C = Middle Plane, D = Nasopharynx

The coordinate reference system in the model is divided into 3 axes. The “z” axis runs from the floor of the nasal cavity to the roof of it. The “y” axis refers the line parallel to the nasal floor while passing along the nasal cavity from nasopharynx to nostril. And “x” axis is the axis that crosses from nasal septum towards the external wall.

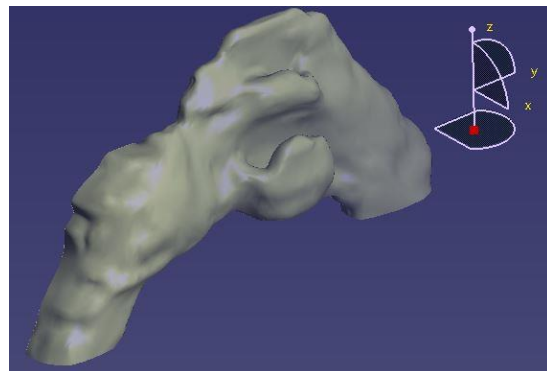


Figure 13: Coordinate reference axes

### 3.2 Experimental Works

The experiments are carried out on the nasal model in order to validate the computational data. PIV method is adapted to enable visualization of the nasal airflow.

### 3.2.1 Experimental Set-Up

The experimental nasal model as shown in Figure 14 is already available from Lee [29]. Due to the aging and current exposure to UV lights, the once clear acrylic (Accura ClearVue Material) turns yellowish.

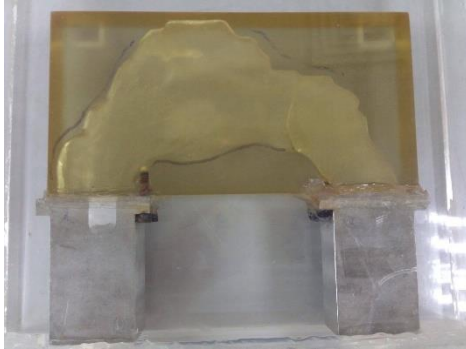
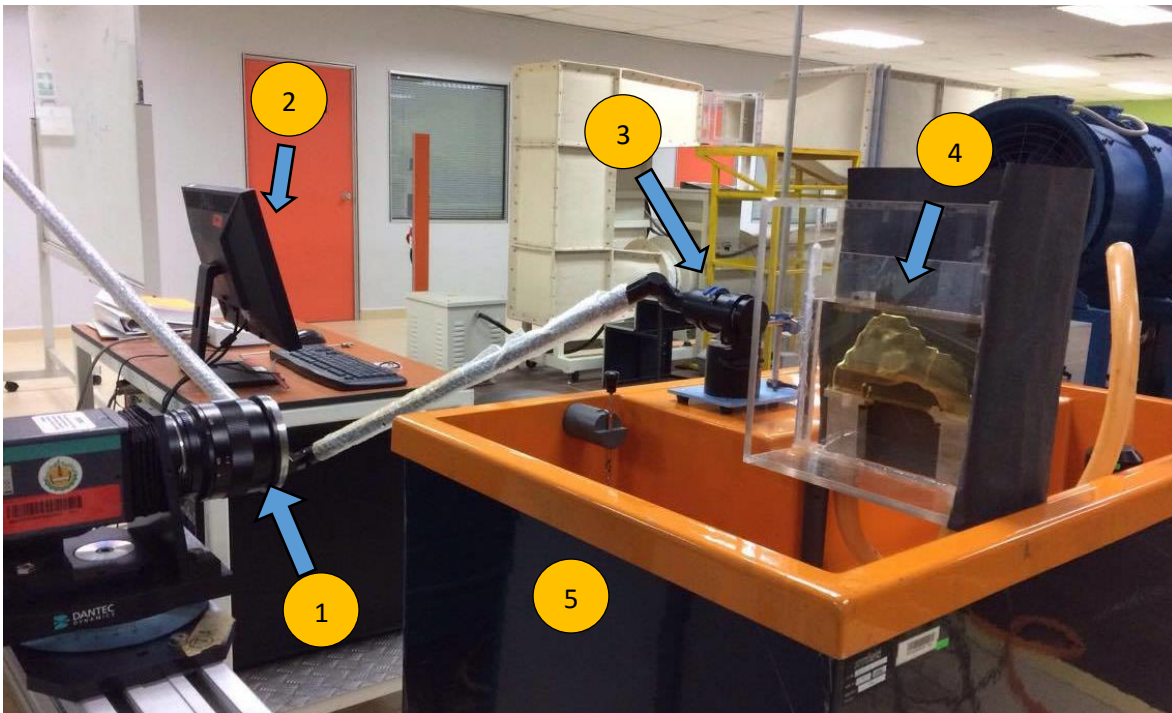


Figure 14: Nasal model from Lee [29]

The experimental set-up includes:

- PIV HiSense MKI camera
- Nd:YAG Laser system
- Computer with Dynamic Studio software
- Hydraulic bench

Figure 15 shows the real arrangement and schematic diagram of the experimental set-up. The nasal model is first immerse in a mixture of glycerol and water with ratio 60:40 inside the Plexiglass container in order to remove the difference in the index of reflectance [10]. The Plexiglass container with the nasal model is placed on top of the water table and a pipe with water pump is attached to the inlet of the model so as to illustrate inspiration flow. Then, the high speed camera is fixed facing the nasal septum wall as the surface is smoother compared to the surface with turbinate. Next, the laser is clamped and placed at the side of the model to let the laser light passed through the model. Different positions of laser light, placed along the “y” and “z” axes are investigated to obtain a better version of images. The outcome shows that images captured when the laser light is placed along “y” axis is clearer. A black-coloured paper is also attached at the Plexiglass container so that to ease the camera in capturing the flow. Instead of using piping system and water pump system separately, a hydraulic bench with water tank, water pump and valve is adapted. This hydraulic bench makes controlling the flow rate easier to handle and takes smaller space for all the equipment [29].



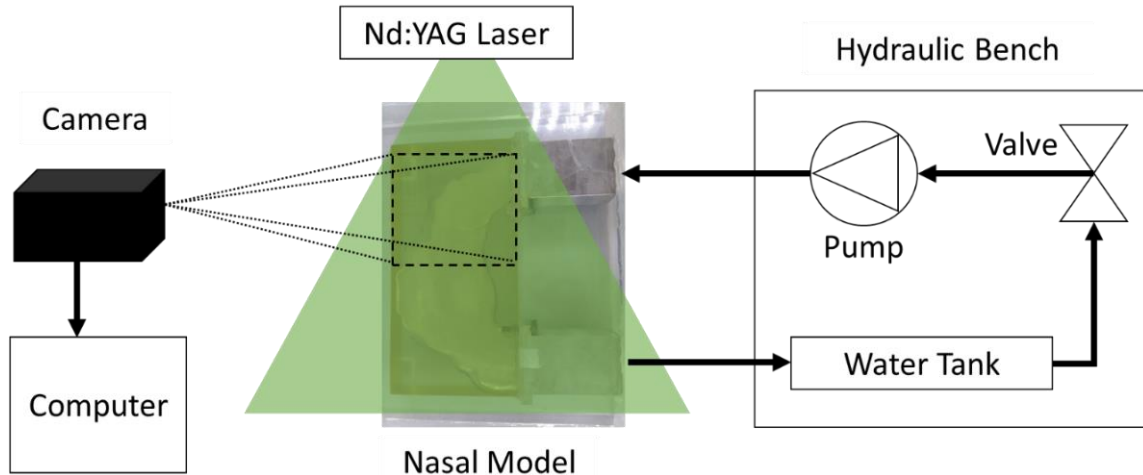


Figure 15: (above) Real experimental set-up: (1) HiSense Camera, (2) Computer system, (3) Nd:YAG Laser system, (4) Nasal Model, (5) Hydraulic bench and (bottom) Schematic diagram of the experimental set-up

### 3.2.2 Selection of Seeding Particles

PIV method depends solely on the scattering particles seeded in the flow. A wide variety of seeding particles is available for PIV experiments. Seeding particles is a necessity to provide velocity information. Hence, it is important to choose the right and compatible seeding. The choice of optimal diameter for seeding particles is a balance between an adequate tracer response in the flow, high signal-to-noise ratio (SNR) for the scattered light signal, and favourably small diameters [28]. However, in this experiment only two types of seeding particles are manipulated, based on previous work by Lee [28]. Lee tested various types of seeding particles and found out that only two of them (as shown in Table 4) are compatible, which are able to follow the flow and depicts good light scattering properties.

Table 4: Types of seeding particles by Lee[29]

Seeding Particles	Particle Diameter ( $\mu\text{m}$ )	Success
Hollow Glass Sphere (HGS)	10	Yes

Polyamide Seeding Particles (PSP)	50	Yes
-----------------------------------	----	-----

In this experiment, both HGS and PSP are tested one after another. The results show that PSP is more suitable due to its larger diameter where it allows the flow to be captured more effectively. Regardless of the two successive tracers, poor results are analyzed due to the unseen particles. Hence, Pliolite AC80 with large-size particles is also being tested despite the density difference between the seeding particles and water. The particles are usually floating or submerged inside the water, thus constant stirring is needed when conducting the experiment. Through this experiment, images with clearer light scattering of particles are captured.

## 4.0 Results and Discussion

### 4.1 Computational Comparison

The validation procedures were obtained from Lee, Wen et al. and Zubair et al. [6, 15, 29]. A laminar model was used to simulate the flow field at flow rates of 4.5 L/min, 7.5 L/min, 10 L/min and 15 L/min while a SST, two-equation

turbulence model was used to simulate the flow field at flow rate of 18 L/min. Comparison of simulation results were carried out for average velocity magnitude, velocity contour and velocity streamline.

#### 4.1.1 Average Velocity Magnitude

Average velocity magnitudes across the nasal cavity from nostril inlet to nasopharynx was obtained at flow rates from 7.5 L/min to 18 L/min. The computational average velocity magnitudes were found to be good agreement with results obtained from previous researchers. Figure 16 and Figure 17 show the average velocity magnitudes at different flow rate of 7.5 L/min and 18 L/min respectively in four different cross sectional planes, namely vestibule, nasal valve, middle plane and nasopharynx.

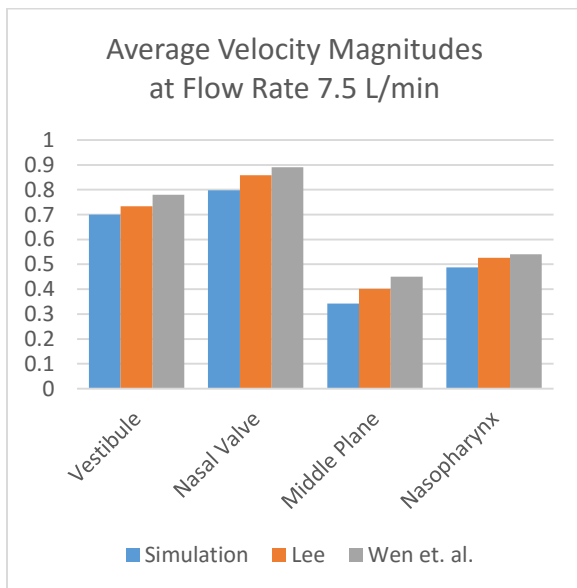


Figure 16: Average velocity magnitudes at flow rate 7.5 L/min in different cross-sectional planes

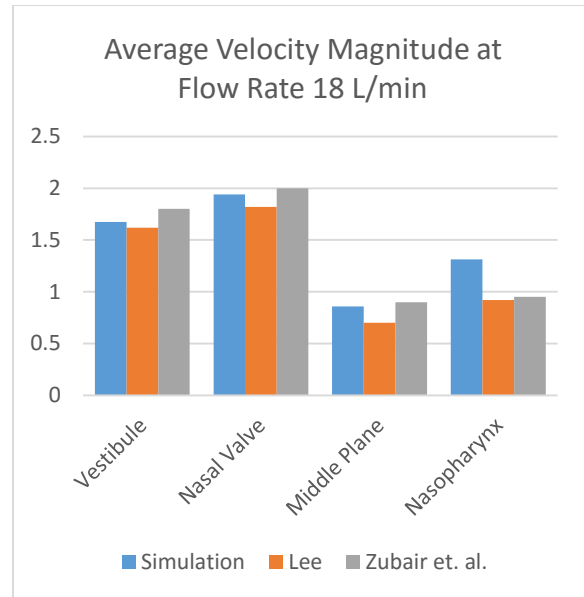


Figure 17: Average velocity magnitudes at flow rate 18 L/min in different cross-sectional planes

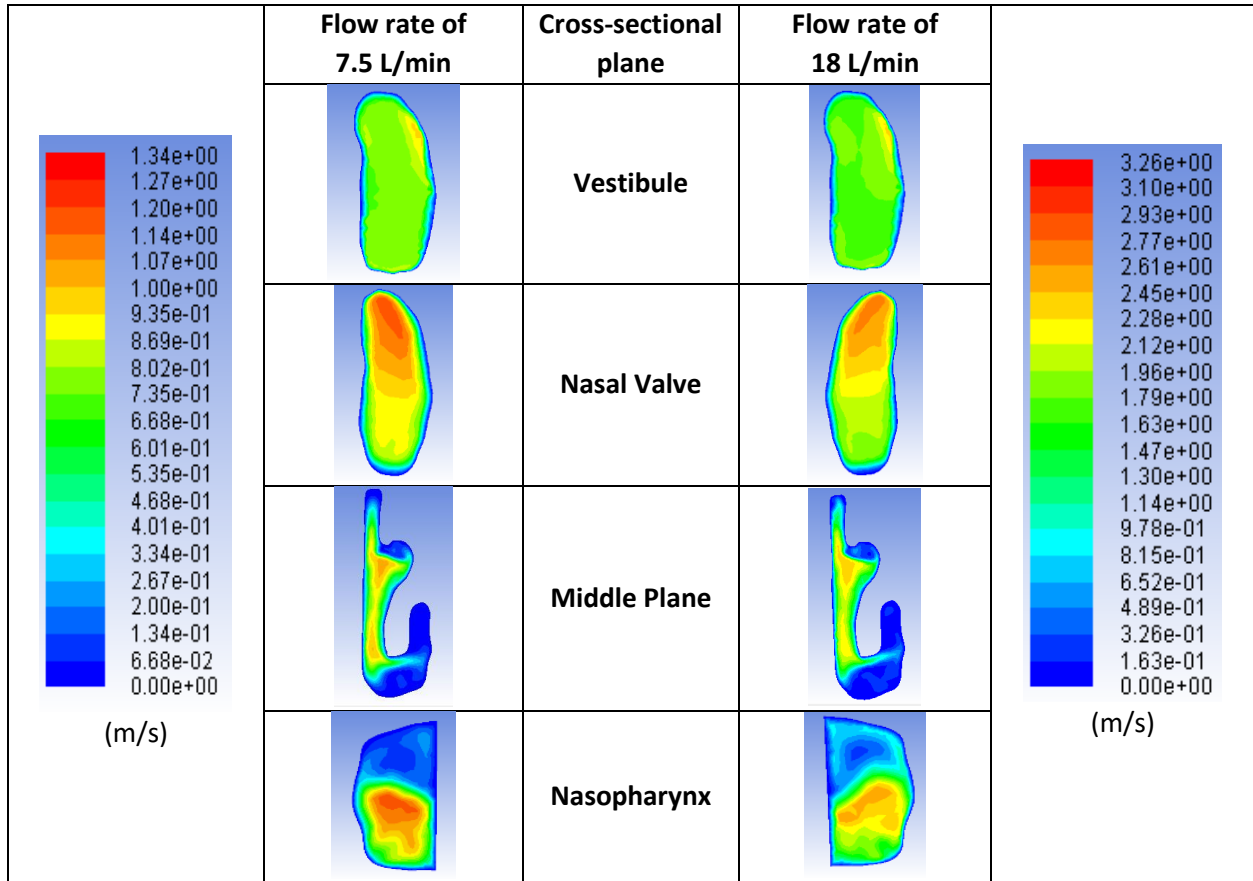
It is observed that the pattern of the graphs is similar for all the models at both 7.5 L/min and 18 L/min flow rates. Nasal valve region is seen to have highest velocity due to the narrower passageway of the nasal cavity. Meanwhile middle plane has the lowest velocity magnitude due to its larger cross-sectional area. The velocity deceleration occurs after the nasal valve region is due to the expansion of cross-sectional area.

However, there are slight deviations of results for both flow rates across the three different models. The differences might be due to different location of cross-sectional planes. Exact position of planes could not be created due to the lack of information such as reference coordinates and plane figures. As a result of deviations in position of planes, different velocity magnitudes are computed as shown in graphs above. Regardless of that, the percentage difference for the models which are more or less of 10%, therefore it is consider quite small and negligible. Hence, it can be said that the computational analysis results are verified as compared to previous researchers' data.



#### 4.1.2 Velocity Contours

Table 5: Velocity contour for flow rate of 7.5 L/min and 18 L/min



As mentioned earlier, the velocity magnitudes computed in Figure 16 and Figure 17 are average values. The graphs do not show how the velocity of the airflow changes across the nasal cavity from nostril to nasopharynx. Hence by comparing velocity contour, clear visualization of the velocity across the four cross-sectional planes are projected.

Referring to Table 5, the velocity contour for flow rate of 7.5 L/min shows the velocity to be at range of 0 – 1.34 m/s. In comparison with higher flow rate of 18 L/min, the highest velocity is 3.26 m/s. It is reasonable and common for turbulent flow to have higher distributed velocities. Both cases show that nasal valve has the highest velocity among the four planes, which validated the hypothesis made earlier where nasal valve has the narrowest passageway

which induces highest velocity. Also, higher velocity is found in the center region of all the planes and decreases towards the nasal wall. This might be due to the viscous nature of airflow which tends to reduce velocities on the nasal wall.

#### 4.1.3 Velocity Streamlines

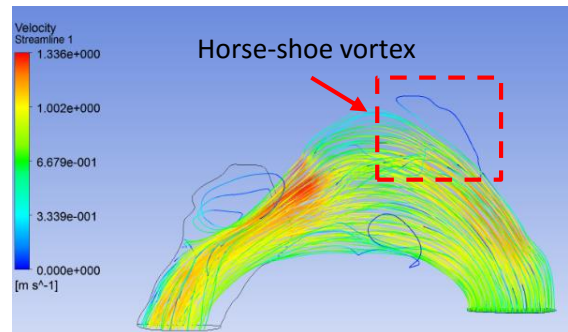


Figure 18: Velocity streamline at flow rate of 7.5 L/min

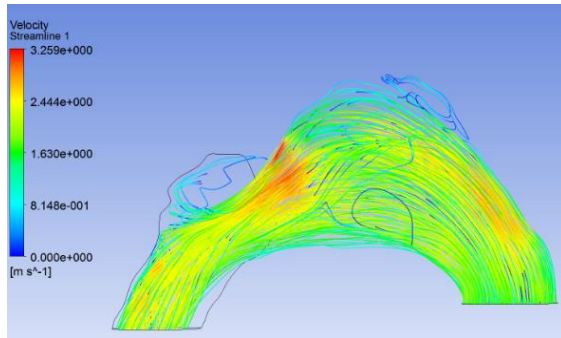


Figure 19: Velocity streamline at flow rate of 18 L/min

Figure 18 and Figure 19 displays the velocity streamlines during inspiration at flow rate of 7.5 L/min and 18 L/min respectively. Streamlines are paths traced out by massless particle moving with the flow. Hence, velocity streamlines can be used to visualize the flow pattern and paths moved by the air particle across the nasal cavity from nostril to nasopharynx. Airflow patterns for the right nasal cavity at flow rate of 7.5 L/min show a formation of horse-shoe shaped vortex at the upper region. This is resulted from the adverse pressure gradient caused by abrupt increase in cross-sectional area from the nasal valve to the main nasal passage [6]. At higher flow rate of 18 L/min, the nature of vortices changed from swirling to combination of swirling and twisting especially in turbinates and nasopharynx.

Observing Figure 19, the convergent-like nasal valve region is seen to have generated two vortices, located in olfactory region and in the lower part of the cavities. The vortex in olfactory region is associated with very low velocities (0.8 m/s, at a flow rate of 18 L/min). This has good agreement with the physiological concept where airflow stays and lingers in the olfactory region for a longer time in order for the olfactory sensory organ to react [21]. Also, the streamlines attributed by flow rate of 18 L/min show a more even velocities and streamlines distribution which is common for turbulent flows. The results obtained depicts that the airflow regime in nasal

cavity relies on the anatomic structure and flow rate [6].

However, the critical flow rate at which the flow regime changes from laminar to turbulent is yet to be defined due to the complexity of the airway [6]. Previous researchers like Bridger and Proctor [37] and Kelly et al. [7] have suggested that a laminar flow regime dominates for low flow rate around 10 L/min. While Churchill et al. [1] demonstrated their result where the rate at which flow switched from transitional to turbulent was around 11 L/min. More recent numerical simulations conducted using realistic nasal airways resulted that the flow is laminar for flow rates below 20 L/min [6].

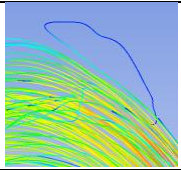
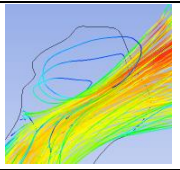
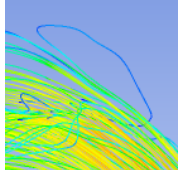
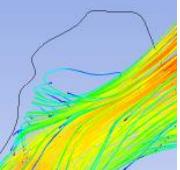
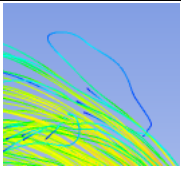
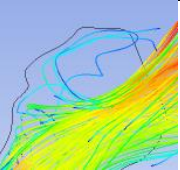
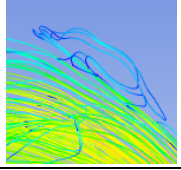
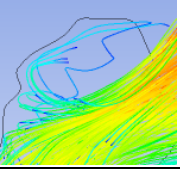
Table 6: Literature survey of airflow regime

Researchers	Laminar	Turbulent
Churchill et al. [1]	< 11 L/min	>11 L/min
Keyhani et al. [13]	< 12 L/min	>12 L/min
Zhu [38]	< 12 L/min	>12 L/min
Zubair et al. [15]	< 15 L/min	>15 L/min
K. Smith [36]	< 15 L/min	>15 L/min
Wen et al. [6]	< 20 L/min	>20 L/min
K. Inthavong et al. [39]	< 20 L/min	>20 L/min

Based on the literature survey on Table 6 , the flow regime whether it is laminar flow or turbulent flow is differentiated via flow rate. According to Zubair et al., the agreement of taking 15 L/min as the boundary where flow is laminar up to 15 L/min and is treated as turbulent flow beyond that flow rate, was based on the calculated Reynolds number. At flow rate 15 L/min, Reynolds number obtained at the nostril inlet was around 1600, while at flow rate 20 L/min, the Reynolds number was 3100 [15]. This is also in good agreement with researchers Churchill et al. that flow will tend to be laminar

at  $Re < 2000$  and at higher values than that the flow will become turbulent [1]. On the other hand, Kalen Smith did figure out the range of flow regime by using turbulent intensity plot using ANSYS, FLUENT [36]. It shows the percentage of turbulence intensity in the nasal cavity model and that was how he managed to differentiate the flow regime.

Table 7: Streamline pattern for two regions in different flow rates

Flow Rate	Region 1	Region 2
7.5 L/min		
10 L/min		
15 L/min		
18 L/min		

As seen in Table 7, streamline pattern for flow rate from 7.5 L/min to 18 L/min are tabulated. The focus is on Region 1, upper region near the inlet of nasal cavity and Region 2, near the nasopharynx region. Previous researchers performed many ways to determine the transition between laminar flow and turbulent flow. However, there is no exact solution to it yet. One of the methods is by visualization and flow streamlines are the path traced out by air particles to show the flow pattern. The simulations tabulated show that in Region 1,

flow recirculation happens at flow rate of 18 L/min, while the flow remains smooth during flow rate of 7.5 L/min, 10 L/min and 15 L/min. At the same time, in Region 2, the flow seems to create more wake and disruptive. Hence, it is reasonable to say that the flow remains laminar from flow rate 7.5 L/min up to 15 L/min and turns turbulent at 18 L/min. This hypothesis is also in good agreement with the literature survey in Table 6 that flow rate 18 L/min is in the range of the proposed transition flow rate which is 15 L/min (Zubair et al. and Kalen Smith) [15, 36] and 20 L/min (Wen et al. and K. Inthavong et al.) [6, 39]. Also, to strengthen the point, Reynolds number is calculated. Reynolds number ( $Re$ ) which is a dimensionless constant used to differentiate the flow regime, are computed. The Reynolds number is given by,

$$Re = \frac{QD}{Av}$$

Where,

$$Q = \text{flow rate of fluid} \left( \frac{m^3}{s} \right)$$

$$D = \text{diameter of pipe (m)}$$

$$v$$

$$= \text{kinematic viscosity of flowing fluid (m}^2/\text{s)}$$

$$A = \text{cross sectional area of pipe (m}^2\text{)}$$

Due to the experimental set-up, the flow of airway is replaced with the mixture of 60% glycerol and 40% water. Hence, in order to match the experimental and computational analysis result, the kinematic viscosity for the mixture is obtained from Chung and Kim, and Kelly et al., which is  $6.55 \times 10^{-6} \text{ m}^2/\text{s}$  at  $27.5 \text{ }^\circ\text{C}$  [7, 9]. The diameter of inlet for the model is 0.025 m. By substituting the constants and values, the corresponding Reynolds number are calculated and tabulated as shown in Table 8 below.

Table 8: Reynolds number calculated corresponding to the flow rate

Flow rate	Reynolds number, Re	Flow Regime
7.5 L/min	972	Laminar
10 L/min	1296	Laminar
15 L/min	1944	Laminar
18 L/min	2332	Turbulent

By comparing the Reynolds number, flow at flow rate 18 L/min is greater than 2000. This has a consensus with the phrase of  $Re > 2000$  will tends to be turbulent by Churchill et al. [1].

#### 4.2 Experimental Comparison

Experimental studies are used to verify the computational results obtained. The experiment is conducted using PIV. PIV is an optical method that is used to visualize flow and capture the velocity maps in flows based on imaging the light scattered by seeding particles in the flow illuminated by a laser light sheet. In order to ensure both computational and experimental results are compatible, similar settings are set including flow rate used, area of interest, and medium of flow.

Flow rate ranging from 4.5 L/min to 7.5 L/min are used to run the experiment. In fact, only results obtained using 4.5 L/min are acceptable. This is because lower flow rate will in not be achievable where the flow is not able to pump through the nasal model due to the gravitational condition. On the other hand, higher flow rate is not favourable because the high speed camera in PIV system is unable to capture the seeding particles in high flow velocity since it can only capture images in 100  $\mu$ s. Figure 20 shows the velocity vector displayed using computational simulation. Due to the complexity of the geometry, the laser light could not illuminate the whole nasal model, hence only a small region of interest (ROI) is captured and analyzed. Therefore, the ROI in Figure 20 is

enlarged and depicted in Figure 21(a) and compared with Figure 21(b) which shows the experimental result analyzed utilizing PIV Lab.

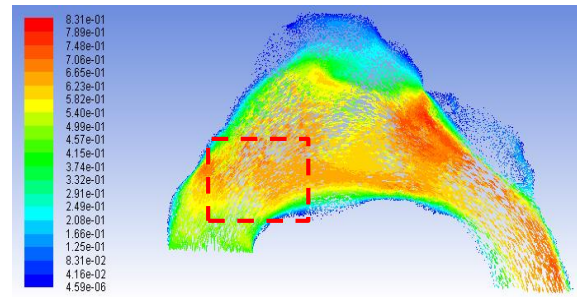
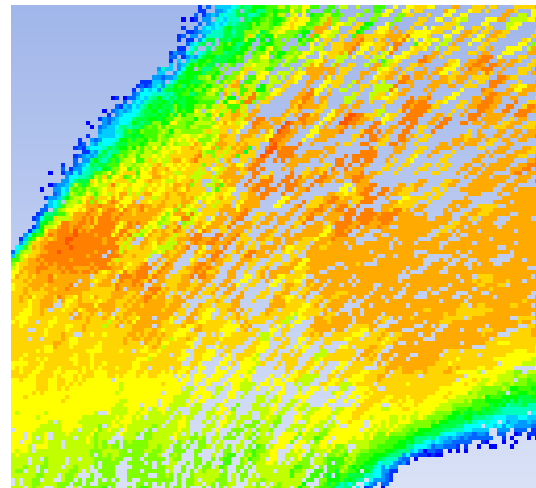
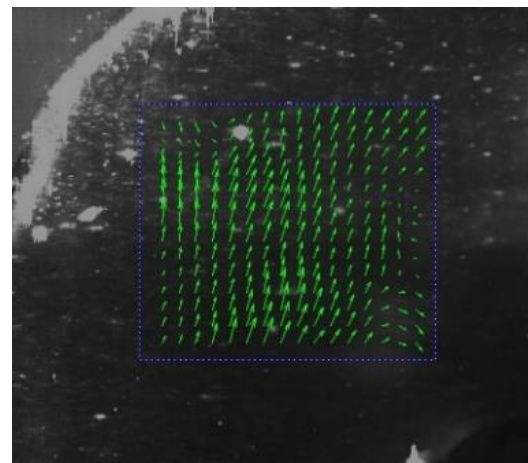


Figure 20: Computational velocity vector at flow rate 4.5 L/min



(a)



(b)

Figure 21: (a) Computational velocity vectors and (b) Experimental velocity vectors at flow rate 4.5 L/min

The velocity vectors in both figures show good accordance where the flow direction changes from vertically upward to slight horizontal following the curvy shape of nasal valve.

However, limited results from experiment are captured due to several factors such as the 3-D geometry of nasal cavity, the material of nasal model, the design of the nasal box, laser profile misalignment, and seeding particles used.

- i. 3-D geometry of nasal cavity – One of the factors is because the nasal geometry is highly complex and curvaceous. The imperfection of the surface such as surface defects causes the laser light to disperse. Dispersion of light has lessened the ability of the laser light to illuminate directly to the seeding particles hence the high speed camera is not able to capture a high quality image. Also, the surfaces which are not flat will tend to act like lenses where it refracts the light illuminated on it thus causes light scattered as well.
- ii. Material of nasal model – Besides that, the nasal model that is made up of Acrylic (Accura ClearVue) material became yellowish due to the aging and constant exposure to UV lights. This also prevents from capturing clear images even though the immersing medium which is mixture of glycerol and water is meant to create a transparent model. The mixture of 59 % glycerol and 41 % water by volume is used as an index of refraction for the nasal model so as to remove refraction of laser light on the nasal model [10].
- iii. The design of the nasal box – The nasal box is made of clear Perspex to hold the nasal model. The wall surface of the Perspex is too thick which has limits the permeability of the laser light, thus lights could not illuminate on

the seeding particles effectively. Meanwhile, the thickness of the wall surface makes the model shows multiple layer of planes which causes the high speed camera to focus on the wrong plane.

- iv. Laser profile misalignment – Other than that, the Nd:YAG laser system faces laser profile misalignment as shown in Figure 22. The mismatch of first and second beam will cause the degradation of quality of result images [40].

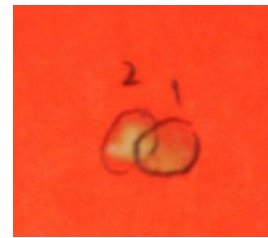


Figure 22: Laser profile misalignment

- v. Selection of seeding particles – Apart from these, the seeding particles play an important role in PIV. Without properly selected seeding particles, the image obtained is just poor in quality [41]. Seeding particles' most important properties are the ability to scatter enough light to create low-noise images as well as their accuracy in following the fluid motion without disrupting the flow [41]. The first seeding particle used the experiment is Hollow Glass Sphere (HGS) with 10  $\mu\text{m}$  diameter as recommended by Lee [29]. However, the particles are too small to be observed and captured by the camera. Thus, Polyamid Seeding Particles (PSP) with 50  $\mu\text{m}$  diameter is used to replace the HGS-10 to enhance the visibility of the particles in the flow. Images captured using PSP-50 has lower noises as compared to images using HGS-10.

## *5.0 Conclusion*

In this paper, the human nasal airway is studied through computational simulation as well as experimental studies. General overview of the nasal airflow patterns is observed after analyzing various data and information collected. Variation of flow rates creates different effects towards the airflow characteristics. Airflow with flow rate ranges from 4.5 L/min to 15 L/min shows that it is smooth and steady which depicts that the flow regime is laminar, while at 18 L/min, the flow started to twist and swirl along the nasal cavity which illustrate turbulence begins. Limitations of experimental model used in this study are reviewed. This problem makes the study of the flow behavior inside the nasal cavity less accurate. Hence, additional effort is required in the future study.

## *6.0 Future Recommendation*

This study only focuses on flow rate ranging from 4.5 L/min to 18 L/min. This small range simulation is insufficient for a good and solid validation purpose. A wider range and smaller interval will deliver better results. Also, the simulations on airflow patterns are only based on low breathing inspiration but simulation on expiration is not performed. Heavy breathing during exercises is also not studied in this case. Thus, information about the non-study cases are not reachable. By doing more simulations on different kind of cases, more data about nasal airflow can be studied and understood.

As for experimental studies, improvements should be made in order to minimize the limitations faced during the experiment. The nasal geometry created using 3D-printing should be designed more smoothly to avoid surface defects and imperfection so that laser light can penetrate through the model without dispersion. Next, the layer of wall surface should be manufactured as thin as

possible so as to allow enough light passing through the model. Clearer version of the material such as clear silicone encased in negative water soluble can also be investigated in future work.

Apart from these, the flow rate for this experiment is limited by the experiment setup and also the restriction of the high speed camera. The orientation of the nasal model is placed where gravitational force could take place. Water could not pump through the nasal model if the flow rate is lowered beyond 4.5 L/min. While for higher flow rate, the camera could not capture the images due to high speed. Therefore, in future work, the orientation or setup of the nasal model can be tried in different ways to manipulate the experiment results. Besides that, different method to measure the instantaneous flow can be studied in future work such as utilizing hot-wire anemometer in a larger scaled nasal model replica to understand the physics of boundary layer transition.

## *Acknowledgement*

I would like to express my profound gratitude to my current supervisor, Dr. Norizham Abdul Razak for his guidance and support in this final year project. Thanks to his valuable wisdom and constantly contributing time to help me grow new understandings. Special thanks to Dr. Lee Chih Fang, who was my previous supervisor, for her encouragement and advice throughout my research journey. I would also wish to thank the technicians and coursemates in School of Aerospace Engineering, USM, for lending their hands in particular occasions. Last but not least, I place on record, my sense of gratitude to one and all who, directly or indirectly, have assisted in my project.

## Reference

1. Churchill, S.E., et al., *Morphological variation and airflow dynamics in the human nose*. American Journal of Human Biology, 2004. **16**(6): p. 625-638.
2. Zhao, K. and P. Dalton, *The way the wind blows: implications of modeling nasal airflow*. Current allergy and asthma reports, 2007. **7**(2): p. 117-125.
3. Liu, Y., et al., *Creation of a standardized geometry of the human nasal cavity*. Journal of Applied Physiology, 2009. **106**(3): p. 784-795.
4. Dohare, P., et al., *Importance of aerodynamics in a human nasal cavity*.
5. Zamankhan, P., et al., *Airflow and deposition of nano-particles in a human nasal cavity*. Aerosol Science and Technology, 2006. **40**(6): p. 463-476.
6. Wen, J., et al. *Airflow patterns in both sides of a realistic human nasal cavity for laminar and turbulent conditions*. in *16th Australasian Fluid Mechanics Conference (AFMC)*. 2007. School of Engineering, The University of Queensland.
7. Kelly, J., A. Prasad, and A.S. Wexler, *Detailed flow patterns in the nasal cavity*. Journal of Applied Physiology, 2000. **89**(1): p. 323-337.
8. Doorly, D., D. Taylor, and R. Schroter, *Mechanics of airflow in the human nasal airways*. Respiratory physiology & neurobiology, 2008. **163**(1): p. 100-110.
9. Chung, S.-K. and S.K. Kim, *Digital particle image velocimetry studies of nasal airflow*. Respiratory physiology & neurobiology, 2008. **163**(1): p. 111-120.
10. Hopkins, L., et al., *Particle image velocimetry measurements in complex geometries*. Experiments in Fluids, 2000. **29**(1): p. 91-95.
11. Schreck, S., et al., *Correlations between flow resistance and geometry in a model of the human nose*. Journal of Applied Physiology, 1993. **75**(4): p. 1767-1775.
12. Weinhold, I. and G. Mlynski, *Numerical simulation of airflow in the human nose*. European Archives of Oto-Rhino-Laryngology and Head & Neck, 2004. **261**(8): p. 452-455.
13. Keyhani, K., P. Scherer, and M. Mozell, *Numerical simulation of airflow in the human nasal cavity*. TRANSACTIONS-AMERICAN SOCIETY OF MECHANICAL ENGINEERS JOURNAL OF BIOMECHANICAL ENGINEERING, 1995. **117**: p. 429-441.
14. Lee, C.F., et al., *Analytical comparisons of standardized nasal cavity*. Journal of Medical Imaging and Health Informatics, 2014. **4**(1): p. 14-20.
15. Zubair, M. and V.N. Riazuddin, *Airflow inside the nasal cavity: visualization using computational fluid dynamics*. Asian Biomed, 2011. **4**(4): p. 657.
16. Chen, X.B., et al. *Numerical simulation for nasal flow with partial inferior turbinatomy-a turbulent model*. in *Biomedical and Pharmaceutical Engineering, 2009. ICBPE'09. International Conference on*. 2009. IEEE.
17. Bailie, N., et al., *An overview of numerical modelling of nasal airflow*. Rhinology, 2006. **44**(1): p. 53.
18. Elad, D., et al., *Analysis of air flow patterns in the human nose*. Medical and Biological Engineering and Computing, 1993. **31**(6): p. 585-592.
19. Shi, H., C. Kleinstreuer, and Z. Zhang, *Laminar airflow and nanoparticle or vapor deposition in a human nasal cavity model*. Journal of biomechanical engineering, 2006. **128**(5): p. 697-706.
20. Kim, S.K. and S.K. Chung, *Investigation on the respiratory airflow in human airway by PIV*. Journal of visualization, 2009. **12**(3): p. 259-266.
21. Croce, C., et al., *In vitro experiments and numerical simulations of airflow in realistic nasal airway geometry*. Annals

- of biomedical engineering, 2006. **34**(6): p. 997-1007.
22. Hahn, I., P.W. Scherer, and M.M. Mozell, *Velocity profiles measured for airflow through a large-scale model of the human nasal cavity*. Journal of Applied Physiology, 1993. **75**(5): p. 2273-2287.
  23. Erny Afiza, Y.T., Taku Atsumi, and Masahiro Iida, *Airflow Patterns within Real and 3D Simplified Models of Nasal Cavities ( I. Experimental Study)*. Proc. Schl. Eng. Tokai Univ. Ser. E., , 2015.
  24. Dombrowski, S., *The Fluid Dynamics of Human Respiration and Olfaction*. Mechanical Engineering, 2012.
  25. Spence, C., N. Buchmann, and M. Jermy, *Unsteady flow in the nasal cavity with high flow therapy measured by stereoscopic PIV*. Experiments in fluids, 2012. **52**(3): p. 569-579.
  26. Stringer, N., et al., *Numerical Comparison of Air Flow Patterns in the Upper Airways of Adults and Neonates*. 2010.
  27. Nayebossadri, S., *Computational and Experimental Study of Nasal cavity Airflow Dynamics*. 2012, Queen Mary University of London.
  28. Melling, A., *Tracer particles and seeding for particle image velocimetry*. Measurement Science and Technology, 1997. **8**(12): p. 1406.
  29. Lee, C.F., *Investigation on Nasal Airflow*, in *Aerospace Engineering*. 2014, Universiti Sains Malaysia.
  30. Castro, R.P., et al., *Computational fluid dynamics simulations of the airflow in the human nasal cavity*. Acta otorrinolaringologica espanola, 2005. **56**(9): p. 403-410.
  31. Lee, C.F., et al., *Standardization of Malaysian adult female nasal cavity*. Computational and mathematical methods in medicine, 2013. **2013**.
  32. Riazuddin, V.N., et al., *Numerical study of inspiratory and expiratory flow in a human nasal cavity*. Journal of Medical and Biological Engineering, 2011. **31**(3): p. 201-206.
  33. Mylavarapu, G., et al., *Validation of computational fluid dynamics methodology used for human upper airway flow simulations*. Journal of biomechanics, 2009. **42**(10): p. 1553-1559.
  34. Segal, R.A., G.M. Kepler, and J.S. Kimbell, *Effects of differences in nasal anatomy on airflow distribution: a comparison of four individuals at rest*. Annals of Biomedical Engineering, 2008. **36**(11): p. 1870-1882.
  35. Liu, Y., et al., *Numerical simulation of aerosol deposition in a 3-D human nasal cavity using RANS, RANS/EIM, and LES*. Journal of Aerosol Science, 2007. **38**(7): p. 683-700.
  36. Smith, K., *Cfd analysis of pressure and flow characteristics of the human nose*. Worcester Polytechnic Institute, 2008.
  37. Bridger, G.P. and D.F. Proctor, *Maximum nasal inspiratory flow and nasal resistance*. Annals of Otology, Rhinology & Laryngology, 1970. **79**(3): p. 481-488.
  38. JIANHUA, Z., *A Numerical Study of Airflow Through Human Upper Airways*. 2012.
  39. Inthavong, K., et al., *A numerical study of spray particle deposition in a human nasal cavity*. Aerosol Science and Technology, 2006. **40**(11): p. 1034-1045.
  40. Grayson, K., I. Marusic, and N. Hutchins, *Analysis of PIV error due to laser light sheet misalignment*. Analysis, 2015. **9**: p. 11.
  41. Adrian, R.J. and J. Westerweel, *Particle image velocimetry*. 2011: Cambridge University Press.